The Functional Asymmetry of *cosN*, the Nicking Site for Bacteriophage λ DNA Packaging, Is Dependent on the Terminase Binding Site, *cosB*†

Julie Qi Hang,‡ Carlos Enrique Catalano,§ and Michael Feiss*,‡

Molecular Biology Program and Department of Microbiology, University of Iowa, Iowa City, Iowa 52242, and Department of Pharmaceutical Sciences, School of Pharmacy, University of Colorado Health Science Center, Denver, Colorado 80262

Received May 31, 2001; Revised Manuscript Received August 15, 2001

ABSTRACT: *cosN* is the site at which terminase, the DNA packaging enzyme of phage λ, introduces staggered nicks into viral concatemeric DNA to initiate genome packaging. Although the nick positions and many of the base pairs of *cosN* show 2-fold rotational symmetry, *cosN* is functionally asymmetric. That is, the *cosN* G_2C mutation in the left half-site (cosNL) causes a strong virus growth defect whereas the symmetrically disposed *cosN* $C_{11}G$ mutation in the right half-site (cosNR) does not affect virus growth. The experiments reported here test the proposal that the genetic asymmetry of *cosN* results from terminase interactions with *cosB*, a binding site to the right of *cosN*. In the presence of *cosB*, the left half-site mutation, *cosN* G_2C, strongly affected the *cos* cleavage reaction, while the symmetric right half-site mutation, *cosN* $C_{11}G$, had little effect. In the absence of *cosB*, the two mutations moderately reduced the rate of *cos* cleavage by the same amount. The results indicated that the functional asymmetry of *cosN* depends on the presence of *cosB*. A model is discussed in which terminase−*cosN* interactions in the nicking complex are assisted by anchoring of terminase to *cosB*.

The DNA replication cycle for the herpesviruses, the poxviruses, and many phages including λ and T3 produces end-to-end multimers of virus chromosomes called concatemers. DNA encapsidation by these viruses involves the specific cutting of concatemers to generate mature virion DNA molecules (*1*−*3*). Terminase enzymes are common to these viruses and are responsible for duplex nicking and packaging of viral DNA into the capsid. λ terminase is a heteromultimer composed of 21-kDa gpNu1[1] and 74-kDa gpA subunits. DNA packaging initiates with the assembly of the terminase subunits at a packaging site, called *cos*, followed by duplex nicking to generate complex I, a stable packaging intermediate. *cos* is composed of three subsites: *cosN*, *cosB*, and *cosQ* (Figure 1A). *cosN* and *cosB* are critical to the assembly of a terminase packaging complex at *cos* and the initiation of genome packaging (*4*, *5*). The *cosQ* subsite plays an important role in the DNA packaging termination (*6*) and will not be discussed in detail here.

cosB is defined functionally as a terminase binding site (*4*, *7*). Within *cosB* there are three distinct gpNu1 binding sites: R1, R2, and R3 (*8*), located in a segment extending from λ bp 53−166 (*4*, *9*, *10*). Terminase binding to the R sites is mediated by a helix−turn−helix DNA binding motif at the amino terminus of gpNu1 (amino acid residues 5−24, A. Becker, cited in reference *11*; *12*; T. de Beer, J. Meyer, M. Ortega, Q. Yang, L. Maes, C. Duffy, N. Berton, J. Sippy, M. Overduin, M. Feiss, and C. E. Catalano, unpublished observations). Between R3 and R2 is I1, a binding site for integration host factor (IHF), the *E. coli* site-specific DNA binding and bending protein (*13*−*18*). The sharp bend imposed by IHF at I1 is proposed to facilitate cooperative interactions between terminase protomers anchored at the R2 and R3 sites (*19*). Between *cosN* and *cosB* is a segment of unknown function called I2 (*14*, *20*).

To the left of *cosB* is *cosN*, defined functionally as the terminase nicking site. *cosN* contains a 22 bp long segment with 10 bp exhibiting 2-fold rotational symmetry. The end points of *cosN* have not been rigorously defined, however. The nick positions are symmetrically disposed within this sequence (Figure 1C). The top strand nick position (N2) is in cosNL, the left *cosN* half-site, and the bottom strand nick position (N1) is in cosNR, the right *cosN* half-site. *cosN*'s 2-fold rotational symmetry suggests that a symmetrically disposed enzyme complex is responsible for duplex nicking activity (*1*, *19*, *21*−*23*).

Despite *cosN*'s 2-fold rotational symmetry, symmetrically placed mutations have unequal effects on phage growth (*24*). Mutations in cosNL have more pronounced phenotypic effects than rotationally symmetric mutations in cosNR. For example, the *cosN* $C_{11}G$ transversion mutation in cosNR (Figure 1C) has no phenotypic effect when present as a single mutation. In contrast, the symmetrically disposed *cosN* G_2C mutation in cosNL has a pronounced phenotypic effect,

† This work is supported by National Institutes of Health Grant GM-51611.

* To whom correspondence should be addressed.

‡ University of Iowa.

§ University of Colorado Health Science Center.

[1] Abbreviations: bp, base pair(s); *cos*, cohesive end site; gpA, the large subunit of terminase; gpNu1, the small subunit of terminase; *cosN*, the site where terminase binds and nicks λ DNA; cosNL, the left *cosN* half-site; cosNR, the right *cosN* half-site; *cosB*, the site where gpNu1 binds; IHF, integration host factor; LA, Luria agar; LB, Luria broth; kb, kilo base pair(s); Kn^R, kanamycin resistance; SOB, Bacto-tryptone-yeast extract−NaCl−$MgSO_4$ medium; Tet^R, tetracycline resistance; TB, TA, and TBSA, tryptone broth, agar, and soft agar, respectively; X-gal, 5-bromo-4-chloro-3-indolyl-β,D-thiogalactopyranoside; IPTG, isopropyl-β,D-thiogalactopyranoside.

10.1021/bi011126r CCC: $20.00
Published on Web 10/12/2001

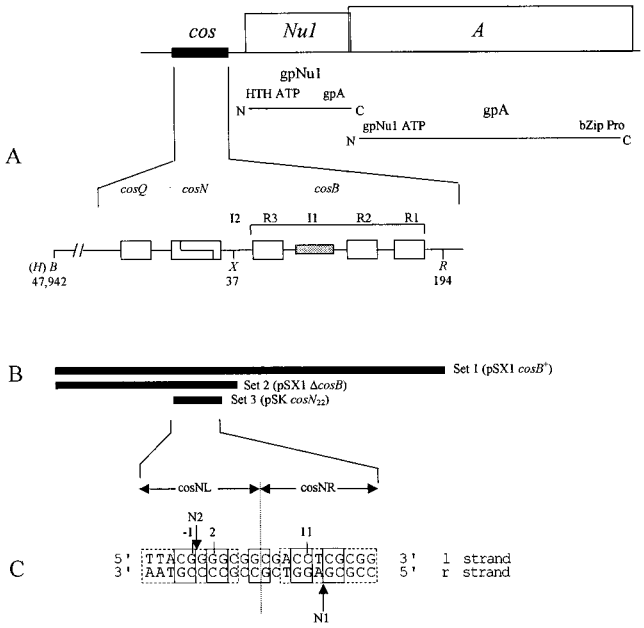

FIGURE 1: Structure of λ *cos*. (A) A schematic diagram of a ~280 bp segment of λ DNA, including *cos*. To the right of *cos* are the *Nu1* and *A* genes that encode the gpNu1 and gpA subunits of terminase, respectively. Expansion: *cos* is tripartite, consisting of the termination signal, *cosQ*, the nicking site, *cosN*, and the terminase binding site, *cosB*. *cosN* is drawn as the rectangle with the potential cohesive ends (*22*). The three R sequences of *cosB* are gpNu1 binding sites (*8, 10*), and I1 is a binding site for IHF, the DNA binding protein of *Escherichia coli* (*14, 15, 17*). I2 is the segment between *cosN* and *cosB*; its function is unclear. The italic letters, *B, X,* and *R*, marked below the *cos* diagram represent the target sites for *Bcl*I, *Xmn*I, and *Eco*RI restriction enzymes at λ bp 47 942 (−560), 37, and 194. (*H*) shows the location of the *Hin*dIII site of the vector's polylinker; this *Hin*dIII site was used in some plasmid constructions. (B) Extent of *cos* carried in the three sets of plasmids used in our *cos* cleavage experiments. The first series of plasmids were pSX1-based and *cosB*$^+$. pSX1 contains the λ DNA segment that starts at a *Bcl*I site located 560 bp upstream of *cosN*, extends through *cos*, to end at an *Eco*RI site at bp 194. The second series of plasmids were Δ*cosB* plasmids containing a 616 bp long λ DNA segment containing *cosQ* and *cosN* but not *cosB*, extending from the *Bcl*I site to the *Xmn*I site; i.e., 560 bp to the left of *cosN* and λ bp 37 to the right of the *cosN* symmetry segment. The third plasmid series are derivatives of the vector pSKII$^+$ bearing the 22 bp *cosN* symmetry segment only. (C) The 22 bp of *cosN*, bisected by its axis of 2-fold rotational symmetry (the vertical dashed line). Boxes denote rotationally symmetrical bp; dashed boxes show purine-pyrimidine symmetry matches. In the *cosN* symmetry segment, base pairs to the left of the symmetry axis, i.e., the left half-site, are called cosNL. Within cosNL, the *l* strand of λ DNA is nicked by terminase, in the nucleotide interval −1/1 (designated N2). In the right *cosN* half-site, cosNR, the *r* strand is nicked in the nucleotide interval 12/13 (designated N1). 2 and 11 are positions of a symmetric pair (base pairs in boldface type) where the G_2C mutation in cosNL and the $C_{11}G$ mutation in cosNR are located.

reducing λ's burst size ~20-fold (*24*). The *cosN* $G_2C-C_{11}G$ double mutation has a more severe effect on virus yield than *cosN* G_2C alone. Similar results were found for mutations at the symmetrical bp positions −1 (bp 48 502 of the λ sequence) and 13 (*24, 25*).

A good correlation was found for mutational effects on virus yield in vivo and *cos* cutting by terminase in vitro, indicating that defective *cosN* cleavage is responsible for the asymmetric phenotypic effects of these mutations. Models for the assembly of a catalytically competent nuclease complex at *cos* suggest that cooperative gpNu1 assembly at *cosB* modulates the assembly of a gpA dimer at *cosN* (*1, 19*). This proposal requires that subunits bound at the two sites interact, and suggests that terminase interactions with *cosB* may be responsible for the functional asymmetry of *cosN* cleavage. In this study, we investigate the effects of *cosB* on the functional asymmetry of *cosN*. *cosB*-deleted substrates with mutations in cosNR and cosNL, alone and in combination, were used as substrates in kinetic studies of *cos* cleavage. Additionally, cleavage of DNA substrates carrying the 22 bp *cosN* symmetry sequence, with or without G_2C or $C_{11}G$ mutations, was investigated to determine if sequences flanking *cosN* are responsible for the observed functional asymmetry in *cos* cleavage (Figure 1B). The implications of these findings for the structure of the nucleoprotein complex of terminase with *cos* subsites are discussed.

Table 1: Strains and Plasmids Used in This Study

strain/plasmid	relevant properties	source/reference
	(A) *E. coli* Strains	
BW313	*dut*1, *ung*1	(*29*)
MF1427	Cla *galK*	(*30*)
MF1478	Cla F$^+$ Str^R $\mu 2^R$ R17^R *thr*$^-$ *leu*$^-$ *xan*$^-$ *his*$^-$ *gal*$^-$	(*31*)
OR1265 (pCM101)	terminase over-production strain	(*32*)
XL1-Blue	*rec*A1 *glnV*44 *lac* [F′ *proAB lacI*^{q}Δ(*lacZ*)m15 Tn10(Tet^R)]	Stratagene, Inc.
	(B) Plasmids	
pSX1	pUC19 containing λ segment from 47 942 to 194	(*24*)
pSX1 *cosN*$_i$	pUC19 containing λ segment from 47 942 to 194, $i = G_2C$, $C_{11}G$, G_2C-$C_{11}G$	(*24*)
pSX1 Δ*cosB* *cosN*$^+$	carries a deletion of *cosB* segment from 37 to 194	this work
pSX1 Δ*cosB* *cosN*$_i$	carries a deletion of *cosB* segment from 37 to 194, $i = G_2C$, $C_{11}G$, G_2C-$C_{11}G$	this work
pSK *cosN*$_{22}$	pSKII$^+$ containing 22 bp of *cosN*$^+$ from −5 to 17	this work
pSK *cosN*$_{22i}$	carries 22 bp of *cosN* from −5 to 17 $i = G_2C$, $C_{11}G$, G_2C-$C_{11}G$	this work

EXPERIMENTAL PROCEDURES

Media, Bacteria, Phages, and Plasmids. TB, TA, and TBSA were prepared as described by Arber et al. (*27*) except that each contained 10 mM $MgSO_4$. LB, LA, and SOB were prepared as described by Sambrook et al. (*28*). Kanamycin, ampicillin, and chloramphenicol were added to media to final concentrations of 50, 100, and 30 μg/mL, respectively. Strains, phages, and plasmids used in this paper are listed in Table 1.

Sequence and Mutation Designations. The phage λ genome numbering convention of Daniels et al. (*26*) is used. Numbering of the λ sequence begins with the first base of the left cohesive end and continues along the top strand in the 5′ to 3′ direction; numbers used in this paper denote bp positions of λ$^+$ DNA (Figure 1C). The top strand is designated the *l*-strand, and the complementary bottom strand is designated *r*. For convenience, we designate base pairs to the left of bp 1 as −1 (λ bp 48 502), −2 (λ bp 48 501), etc. *cosN* G_2C and *cosN* $C_{11}G$ are transversion mutations at

positions 2 and 11 of λ cosNL and cosNR, respectively (see Figure 1C). *cosN* $G_2C-C_{11}G$ carries both mutations.

Enzymes and General DNA Recombinant Techniques. Restriction enzymes, bacteriophage T4 DNA ligase, and the Klenow fragment of DNA polymerase I were purchased from New England Biolabs and Boehringer-Mannheim, and were used according to the suppliers' recommendations. Plasmid DNA was purified using the Qiagen Plasmid Maxi Kit. DNA restriction fragments from agarose gels were purified using the Qiagen Quick Gel Extraction Kit. Transformations were performed using the procedure of Hanahan (*33*). Radionucleotides were obtained from Amersham Pharmaceuticals.

cosB$^+$ *Substrates.* pSX1 contains wild-type λ DNA extending from λ bp 47 942 through *cos* to 194, cloned into a pUC19 background (Figure 1B) (*24*). Derivatives of pSX1 carrying the *cosN* G_2C, *cosN* $C_{11}G$, and *cosN* $G_2C-C_{11}G$ mutations were described previously (*24*).

Construction of Δ*cosB Substrates*. Cosmid pSX1 and derivatives carrying *cosN* G_2C, *cosN* $C_{11}G$, or *cosN* $G_2C-C_{11}G$ mutations were used to generate the corresponding Δ*cosB* substrates, as follows. pSX1 contains an *Xmn*I site between *cosN* and *cosB* (Figure 1A). The *Xmn*I restriction enzyme cuts the site between λ bp 37 and 38, so *cosB* can be deleted by removing λ DNA to the right of the *Xmn*I site. Accordingly, the λ DNA segment extending from a *Bcl*I site at λ bp 47 942 to the *Xmn*I site was excised from the pSX1 plasmid series by digesting with *Hin*dIII and *Xmn*I. *Hin*dIII cuts a *Hin*dIII site in the pSX1 polylinker located to the left of the λ DNA insert. These 616 bp long segments, containing *cosQ* and *cosN* but not *cosB*, were ligated into *Hin*dIII-, *Sma*I-digested pUC19. The resulting plasmids, called Δ*cosB* plasmids, were used to transform XL1-Blue cells and subsequently used as substrates for *cos* cleavage. Note that this Δ*cosB* series of plasmids contains λ sequences flanking the *cosN* symmetry segment, since the λ segment extends rightward from the *Bcl*I site at 47 942 through *cosN* to the *Xmn*I site at λ bp 37.

Construction of $cosN_{22}$ *Substrates*. *cos* cleavage substrates containing an isolated 22 bp *cosN* subsite (λ bp 48 498 to 17) were constructed by insertion of duplex synthetic oligonucleotides into pSKII$^+$. The oligonucleotides contained *Hin*dIII and *Xba*I ends, and were wild-type, or contained the *cosN* mutations shown below as boldface and underlined:

$cosN_{22}$	5'-CTAGTTACGGGGCGGCGACCTCGCGGCTA-3' AATGCCCCGCCGCTGGAGCGCCGATTCGA
$cosN_{22}$ G_2C	5'-CTAGTTACGG**C**GCGGCGACCTCGCGGCTA-3' AATGCC**G**CGCCGCTGGAGCGCCGATTCGA
$cosN_{22}$ C_{11}	5'-CTAGTTACGGGGCGGCGAC**G**TCGCGGCTA-3' AATGCCCCGCCGCTG**C**AGCGCCGATTCGA
$cosN_{22}$ $G_2C-C_{11}G$	5'-CTAGTTACGG**C**GCGGCGAC**G**TCGCGGCTA-3' AATGCC**G**CGCCGCTG**C**AGCGCCGATTCGA

The duplexes were ligated into *Hin*dIII/*Xba*I-digested pSKII$^+$, and the ligation mixtures were transformed into XL1-Blue cells. White colonies growing on LA plates containing 0.024% X-gal (w/v) and 0.2 mM IPTG were isolated, and the presence of the appropriate insert was verified by DNA sequencing.

Protein Purification. Terminase extracts were prepared from MF1427 (pCM101) according to the method of Chow et al. (*32*). Terminase was purified by a modification (*34*) of the method of Tomka and Catalano (*35*). IHF was purified by Young Hwang of our laboratory (*34*).

cos Cleavage Reactions. cos cleavage assays were performed using the protocol of Chow et al. (*32*). The reactions (20 μL) contained 30 mM Tris-HCl (pH 9.0), 10 mM $MgCl_2$, 3 mM spermidine, 6 mM putrescine, 7 mM β-mercaptoethanol, 1.5 mM EDTA, 1.5 mM ATP, 10 nM IHF, and 70 nM *Bsa*I-linearized DNA substrate. The reaction was initiated with the addition of terminase to 150 nM and incubated at room temperature (~22 °C) for the times indicated in the figure legends. The terminase concentration is expressed as the molarity of terminase protomers with the composition of gpA_1:$gpNu1_2$ (*35*). A 2 μL aliquot of agarose gel loading buffer (50% glycerol, 0.1 M EDTA, 1% SDS, and 0.1% bromophenol blue) was added to stop the reaction. The samples were heated at 65 °C for 10 min to separate cohesive ends prior to fractionation of the products by 1% agarose gel electrophoresis. Following electrophoresis, the DNA was transferred onto a GeneScreen Plus (New England Nuclear) membrane. DNA hybridizations were performed using an appropriate [α-^{32}P]dCTP-labeled probe, and the products were analyzed by scanning in a Packard Instrument phosphorimager apparatus. The *cosB*$^+$ and Δ*cosB* substrate DNAs were linearized, pUC19-based cosmids containing the λ DNA segments shown in Figure 1B. The cosmids were linearized with *Bsa*I restriction enzyme prior to use as substrates in *cos* cleavage reactions. Cleavage of these linear DNAs at *cos* produced 1.51 and 1.91 kb product fragments. The $cosN_{22}$ substrate DNAs were linearized, pSKII$^+$-based cosmids containing the λ DNA segments shown in Figure 1B. The cosmids were linearized with *Bsa*I restriction enzyme prior to use as substrates in *cos* cleavage reactions. Cleavage of these linear DNAs at *cos* produced 1.73 and 1.95 kb product fragments.

Analysis of Apparent DNA Binding Affinity. We used initial rate measurements to determine the concentration of DNA required to maximally stimulate the *cos* cleavage reaction with each of the DNA substrates.[2] The reactions were carried out at room temperature (~22 °C) using 150 nM terminase and the DNA concentrations indicated in the figure legends; *cos* cleavage measurements were made at multiple time points during the period of approximate linearity. We define k_{max} as the maximal initial rate obtained at saturating DNA concentrations.

Kinetic Analysis. The reaction time course was analyzed as described previously (*35*). Each data set was analyzed according to both eq 1 and eq 2, which describe monophasic and biphasic reaction time courses, respectively:

$$\text{Products} = A - B^*\exp(-k_{mono}\tau) \quad (1)$$

$$\text{Products} = A - C^*\exp(-k_{slow}\tau) - D^*\exp(-k_{fast}\tau) \quad (2)$$

where Products refers to the fraction of DNA digested at time τ and A is the extent of the reaction at $\tau = \infty$. k_{mono} is the rate constant obtained from fitting the data to eq 1. C and D describe the fraction of the observed rate associated

[2] The nuclease reaction is stoichiometric rather than catalytic under the conditions used here (*35*), and the reaction is not strictly linear (*35*). Nevertheless, the reactions approximated linearity for the first 2 and 5 min for *cosB*$^+$- and *cosB*-deleted substrates, respectively.

with the slow and fast phases, respectively, and k_{slow} and k_{fast} represent the observed rate constants for the reaction's slow and fast phases, respectively. The indicated constants were determined by nonlinear regression analysis of the experimental data using the SigmaPlot scientific graphing software (version 5.0, SPSS Inc., Chicago, IL) as described previously (*35*). A monoexponential curve function was deemed appropriate to describe the data if (1) the values of the rate constants, k_{slow} and k_{fast}, obtained by nonlinear regression analysis of the data to eq 2 differed by less than 10-fold, and (2) the Ψ^2 value obtained from fitting to eq 1 was within an order of magnitude of that obtained from fitting to eq 2.

RESULTS

Symmetric Mutations in cosN Have Asymmetric Effects on cos Cleavage. Previous in vitro *cos* cleavage experiments using crude terminase preparations showed that the *cosN* G_2C mutation in cosNL caused a cleavage defect, but the symmetrical *cosN* $C_{11}G$ mutation in cosNR did not (*24*). Furthermore, *cos* cleavage defects correlated well with the mutational effects on burst size, DNA packaging, and prohead utilization. These results suggested that the *cos* cleavage defect accounted for the phenotypes of the *cosN* mutants. To study in detail the effects of these mutations on the nuclease activity of λ terminase, *cos* cleavage reactions were performed using purified enzyme in a defined biochemical reaction mixture.

We first examined apparent binding interactions between terminase and each of the DNA substrates by measuring the initial rates of *cos* cleavage as a function of substrate concentration. The *cosN* $C_{11}G$ mutation had little effect on apparent DNA binding and/or the rate of *cos* cleavage relative to wild-type DNA (Figure 2A). The initial rates were similar for both substrates at all of the DNA concentrations examined, and the apparent half-saturating concentrations of DNA ($C_{1/2,app}$) were essentially identical for both substrates (Table 2). In contrast, the symmetric *cosN* G_2C mutation had dramatic effects, increasing the $C_{1/2,app}$ more than 4-fold. Moreover, this mutation decreased the maximal observed rate (k_{max}) more than 2-fold (Figure 2A, Table 2). Similar, though more severe, effects were observed with the *cosN* $G_2C-C_{11}G$ double mutant (Figure 2A, Table 2). These results agree with those of Higgins and Becker (*25*, *36*), who demonstrated that the *cosN* $G_{-1}T$ transversion mutation in cosNL caused a 3-fold decrease in nicking at the N2 position, while the symmetric *cosN* $C_{13}G$ mutation in cosNR had no effect on nicking at N1.

We next examined the time course for *cos* cleavage using each of the DNA substrates described above. We have previously demonstrated that the *cos* cleavage reaction time course is biphasic under these conditions, exhibiting fast and slow phases (*35*). The reaction time course for the *cosN* $C_{11}G$ mutant DNA substrate was essentially identical to that for the wild-type *cosN*$^+$ DNA substrate (Figure 2B); both substrates exhibited a biphasic time course yielding the observed rate constants shown in Table 3. We note that the kinetic constants obtained here are similar to those published previously (*35*). The *cosN* G_2C mutation had pronounced effects on the *cos* cleavage reaction, yielding a monophasic time course and substantially limited reaction extent (Figure 2B). The observed rate of this monophasic reaction, k_{mono}, is similar to the k_{slow} observed with the wild-type substrate. Similar results were observed with the *cosN* $G_2C-C_{11}G$ double mutant DNA. We note that the time course studies

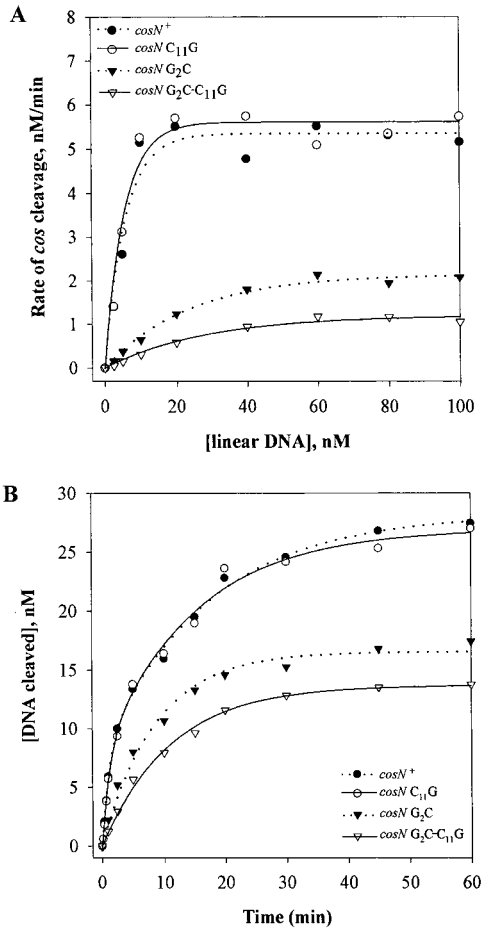

FIGURE 2: Effects of *cosN* mutations on *cos* cleavage. Reactions used *Bsa*I-linearized *cosB*$^+$ substrates (Table 1). The reaction conditions were as described under Experimental Procedures. (A) Dependence of initial rate of *cos* cleavage on substrate DNA concentration. (B) Time course of *cos* cleavage with *cosB*$^+$ substrates at 70 nM. Data points represent the average value of three separate experiments. The curves show the best fit generated by nonlinear regression analysis of the data as described under Experimental Procedures.

Table 2: Effect of DNA Concentration on the *cos* Cleavage Reaction[a]

DNA substrates	$C_{1/2,app}$[b] (nM)	k_{max}[c] (nM/min)
(a) *cosB*$^+$ Substrates		
cosN$^+$[d]	4.00 ± 0.95	5.35 ± 0.24
cosN $C_{11}G$	3.85 ± 0.77	5.61 ± 0.21
cosN G_2C	16.5 ± 1.98	2.14 ± 0.08
cosN $G_2C-C_{11}G$	19.6 ± 3.82	1.20 ± 0.07
(b) Δ*cosB* Substrates		
Δ*cosB cosN*$^+$[d]	7.18 ± 1.27	1.05 ± 0.04
Δ*cosB cosN* $C_{11}G$	5.92 ± 1.15	0.69 ± 0.03
Δ*cosB cosN* G_2C	6.48 ± 0.72	0.61 ± 0.02
Δ*cosB cosN* $G_2C-C_{11}G$	22.4 ± 4.78	0.072 ± 0.005

[a] The data presented in Figures 2A and 3A were analyzed as described under Experimental Procedures. The results are presented in sections (a) and (b) of the table, respectively. [b] $C_{1/2,app}$ is the DNA concentration required to half-maximally stimulate the reaction. [c] k_{max} is the maximal initial rate of *cos* cleavage at saturating DNA concentrations. [d] *cosN*$^+$ represents DNA containing wild-type *cosN*.

Table 3: Kinetic Analysis of the *cos* Cleavage Reaction[a]

DNA substrates	k_{mono} (min^{-1})	k_{fast} (min^{-1})	k_{slow} (min^{-1})
(a) *cosB*$^+$ Substrates			
cosN$^{+\,c}$		0.886	0.058
cosN $C_{11}G$		0.794	0.067
cosN G_2C	0.116	*b*	*b*
cosN G_2C-$C_{11}G$	0.095	*b*	*b*
(b) Δ*cosB* Substrates			
Δ*cosB cosN*$^{+\,c}$	0.102	*b*	*b*
Δ*cosB cosN* $C_{11}G$	0.086	*b*	*b*
Δ*cosB cosN* G_2C	0.079	*b*	*b*
Δ*cosB cosN* G_2C-$C_{11}G$	0.016	*b*	*b*
(c) $cosN_{22}$ Substrates			
$cosN_{22}{}^{+\,c}$	0.060	*b*	*b*
$cosN_{22}$ $C_{11}G$	0.039	*b*	*b*
$cosN_{22}$ G_2C	0.043	*b*	*b*
$cosN_{22}$ G_2C-$C_{11}G$	0.008	*b*	*b*

[a] The data presented in Figures 2B, 3B, and 4 were analyzed as described under Experimental Procedures. The results are presented in sections (a), (b), and (c) of the table, respectively. [b] These data were well described by eq 1, and k_{mono} is the observed rate constant for the monophasic reaction. k_{fast} and k_{slow} are the observed rate constants for the fast and slow phases of the biphasic time courses, respectively. [c] *cosN*$^+$ represents DNA containing the wild-type *cosN* sequence.

clearly demonstrate that, compared to wild-type and *cosN* $C_{11}G$ mutant DNA substrates, the *cosN* G_2C mutation significantly limits the reaction extent. The reason for this is not clear.

Asymmetric Effects of cosN Mutations on cos Cleavage: Role of cosB. Previous studies have demonstrated that *cosB* is required for efficient *cos* cleavage (*36*, *37*). Introduction of point mutations into each of the R elements of *cosB* ($R3^-R2^-R1^-$ triple point mutant) and/or the complete deletion of *cosB* (Δ*cosB* mutant) decreased the overall extent of duplex nicking (*25*, *38*). With both substrates, cosNL nicking at N2 nicking was more severely affected than was cosNR nicking. These studies suggest that *cosB* contributes to the observed asymmetric nicking of the two *cosN* half-sites. To examine further the role of *cosB* in the functional asymmetry of *cosN*, we examined the effects of *cosN* mutations in a Δ*cosB* background. We reasoned that if *cosB* is responsible for the observed asymmetry in the nicking reaction, deletion of this region should yield substrates in which mutations in each half-site should have equal effects on *cosN* cleavage.

We first examined apparent binding interactions between terminase and a Δ*cosB* DNA substrate containing the wild-type *cosN* sequence (*cosN*$^+$, see Figure 1B,C). Though deletion of *cosB* modestly increased $C_{1/2,app}$, it strongly affected the *cos* cleavage reaction, reducing k_{max} 5-fold (Figure 3A; Table 2). These results are consistent with *cosB*'s known function of promoting the efficiency of *cos* cleavage (*36*, *38*).

We next examined the effect of introducing the *cosN* G_2C or *cosN* $C_{11}G$ mutations into the Δ*cosB* substrate. Neither mutation affected the apparent binding interactions beyond that observed for deletion of *cosB* alone (Figure 3A, Table 2). Introduction of the *cosN* C_2G mutation into a Δ*cosB* background decreased k_{max}, though not as strongly as was observed in the presence of *cosB* (see Table 2). Introduction of the symmetric *cosN* $G_{11}C$ mutation similarly decreased k_{max}, a result in stark contrast to that obtained in the

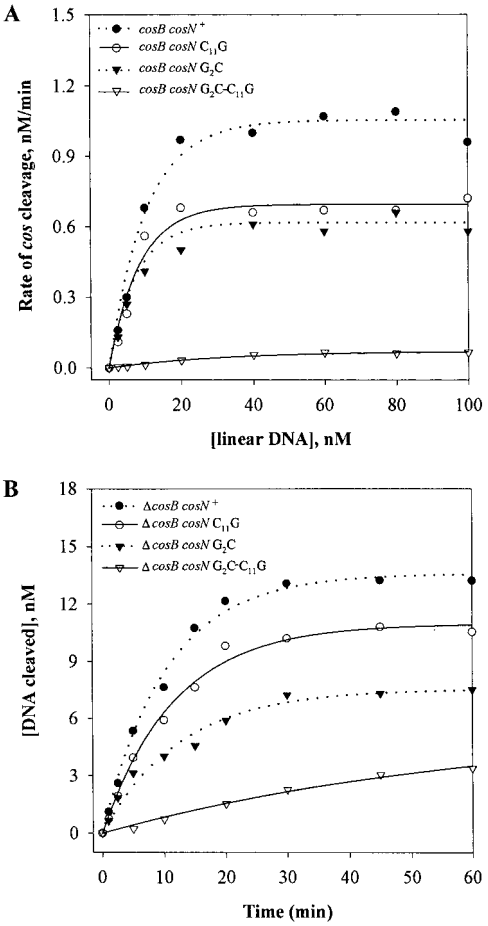

FIGURE 3: Effects of deletion of *cosB* on *cos* cleavage. Reactions used *Bsa*I-linearized pSX1 Δ*cosB* and its derivatives pSX1 Δ*cosB* $cosN_i$ as DNA substrates (Table 1). The reaction conditions were as described under Experimental Procedures. (A) Dependence of initial rate of *cos* cleavage on substrate DNA concentration. (B) Time course of *cos* cleavage with Δ*cosB* substrates at 70 nM. The data points represent the average value of three separate experiments. The curves show the best fit generated by nonlinear regression analysis of the data as described under Experimental Procedures.

presence of *cosB* (compare Figure 3A with Figure 2A). Introduction of both mutations into a Δ*cosB* background had a striking effect on both $C_{1/2,app}$ and k_{max}, again contrasting the results obtained with the *cosB*$^+$ substrates (compare Figure 3A with Figure 2A; see Table 2). These results indicate that *cosB* plays a dominant role in the functional asymmetry of *cosN*.

Finally, we examined the *cos* cleavage time course using the Δ*cosB* substrates. These studies revealed that deletion of *cosB* yielded monophasic reaction time courses for all of the substrates examined (Figure 3B, Table 3). The observed rates of these reactions are similar to the k_{slow} observed with the wild-type (*cosN*$^+$, *cosB*$^+$) DNA substrate. Consistent with the studies described above, the observed rates of *cos* cleavage were similar for the Δ*cosB cosN* G_2C and Δ*cosB cosN* $C_{11}G$ substrates, though the former mutation's effect was slightly greater. Moreover, introduction of both mutations into a Δ*cosB* substrate has significantly greater effects than either one alone (Figure 3A).

Deletion of λ Flanking Sequences Eliminates Asymmetry. The Δ*cosB* substrates used in the previous section contained λ sequence in addition to *cosN*. To investigate the effects of

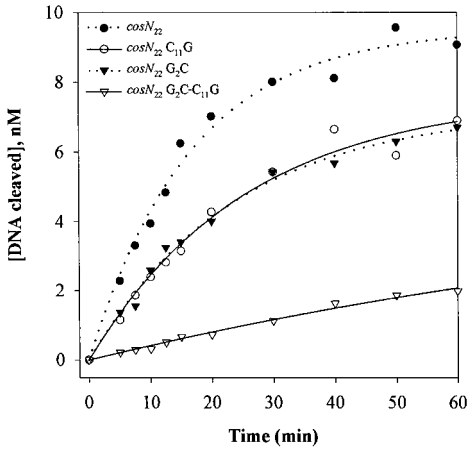

FIGURE 4: Time course of *cos* cleavage of a minimal *cosN* substrate. Reactions used *Bsa*I-linearized pSK $cosN_{22}$ and its $cosN_{22i}$ derivatives as DNA substrates (Table 1). The DNA concentration was at 50 nM and was saturating for all the substrates (data not shown). Each data point represents the average value of two separate experiments. The curves are the best fit generated by nonlinear regression analysis of the data as described under Experimental Procedures.

the sequences adjacent to *cosN*, DNA substrates containing the isolated 22 bp *cosN* symmetry sequences (wild-type and mutant) were constructed (Figure 1B). As with the Δ*cosB* substrates, the reaction time courses for all of the isolated *cosN* substrates were monophasic (Figure 4). In each case, the observed rate of *cos* cleavage was roughly half that observed with the corresponding Δ*cosB* substrate (see Table 3). Significantly, the time courses for cleavage of the $cosN_{22}$ G_2C and $cosN_{22}$ $C_{11}G$ substrates were virtually identical, demonstrating that the asymmetry of *cos* cleavage was completely abolished in the absence of flanking λ sequences.

DISCUSSION

Asymmetry in the cos Cleavage Reaction. The *cosN* and *cosB* subsites are critical to the assembly of a terminase packaging complex at *cos* and to the initiation of genome packaging (*4*, *7*). The in vitro *cos* cleavage assay used in this study corresponds to the duplex nicking reaction for packaging initiation, and a kinetic model for this reaction is presented in Scheme 1 .

In this model, terminase's gpA and gpNu1 subunits assemble at *cosN* and *cosB*, respectively (shown as $T{\cdot}D_{cos}$ in the scheme). ATP promotes a conformational reorganization of the protein subunits to yield a catalytically competent nuclease complex of high fidelity ($T^*{\cdot}D_{cos}$) (*5*). Magnesium-dependent nicking of the *r*-strand at N1 ($T^*{\cdot}D_{L-R}$) is followed by *l*-strand nicking at N2 to yield the nicked, annealed duplex ($T^*{\cdot}D_L{\cdot}D_R$). Finally, ATPase-dependent strand separation yields complex I ($T{\cdot}D_L$), a nucleoprotein complex composed of the terminase subunits bound to and protecting the mature left end of the first genome to be packaged. This packaging intermediate, known as complex I, is unusually stable in the absence of procapsids. It has been isolated from *E. coli* cells infected with capsid-deficient virus (*39*), and has been characterized in vitro (*5*). The prolonged half-life of complex I ($T_{1/2} > 8$ h in the absence of proheads) results in a stoichiometric rather than catalytic nuclease reaction under the assay conditions utilized in this study (*5*).

Our data clearly demonstrate that in an otherwise wild-type *cos* background, introduction of the point mutation *cosN* $C_{11}G$ into cosNR has little effect on the *cos* cleavage reaction. Conversely, the symmetrically disposed mutation *cosN* G_2C in cosNL has strong effects. We note several effects of the *cosN* G_2C mutation on the *cos* cleavage reaction.

First, higher concentrations of *cosN* G_2C DNA are required to stimulate nuclease activity when compared to wild-type DNA. This could indicate that intrinsic binding interactions between gpA and the mutant cosNL half-site are attenuated, resulting in an increased "K_D". Terminase assembly at *cos* is complex, however, and cannot be interpreted as a simple, reversible binding interaction. Rather, assembly requires that the gpA and gpNu1 subunits cooperatively bind at *cosN* and *cosB*, respectively (Scheme 1, step 1) (*40*). Nevertheless, the initial interactions are concentration-dependent, and the decrease in apparent binding affinity for this substrate may reflect altered gpA·cosNL binding interactions.

A second effect of the cosNL mutation is that the maximal nuclease rate observed at saturating DNA concentrations is significantly slower compared to that observed with wild-type and *cosN* $C_{11}G$ substrates. Impaired gpA·cosNL binding interactions may play a role here as well. In this case, mutations in cosNL would affect the conformational change step (Scheme 1, step 2). The conformational change to a catalytically competent prenicking complex requires a reorganization of the protein subunits assembled at *cos*. DNase footprinting studies have demonstrated a major ATP-driven change in the protection pattern surrounding *cosN*, presumably due to increased gpA binding interactions (*42*). It is thus feasible that the conformational change step requires alteration of the binding contacts between a gpA subunit and cosNL, and that these interactions are impaired in the *cosN* G_2C mutant substrate.

A third effect of the cosNL mutation is that the nuclease time course is monophasic, in contrast to the biphasic reaction time course observed with wild-type and *cosN* $C_{11}G$ substrates. We have previously demonstrated biphasic kinetics and have suggested that the slow phase (k_{slow}) is dominated by protein assembly steps (*35*, *41*). Importantly, the monophasic rate constant obtained with the *cosN* G_2C substrate is similar to k_{slow}, suggesting that protein assembly steps are always rate-limiting. This could result from impaired gpA binding interactions with the mutant cosNL half-site.

The increase in apparent K_D, the decrease in nuclease rate, and the monophasic reaction time course observed with the *cosN* G_2C substrate all may be explained by impaired gpA binding interactions with the mutant cosNL half-site. This may be an oversimplification, however. It is feasible that the *cosN* G_2C mutation directly affects one or both of the nicking steps (Scheme 1, steps 3 and 4). If the mutation affects duplex nicking such that this becomes the rate-limiting step of the reaction, the observed rate would be slower compared to wild-type DNA, and the reaction would exhibit a monophasic time course. This is exactly what is observed. This mechanism would also provide an explanation for the fourth effect of the cosNL G_2C mutation; that is, the extent of the nuclease reaction is decreased by roughly 50%. This suggests, but does not prove, that nicking at the N2 site is affected by the cosNL mutation, and that this leads to a "dead-end" complex that is not detected in our assay. A likely candidate for this aborted complex is the protein-bound

Scheme 1: Kinetic Model for the *cos* Cleavage Reaction

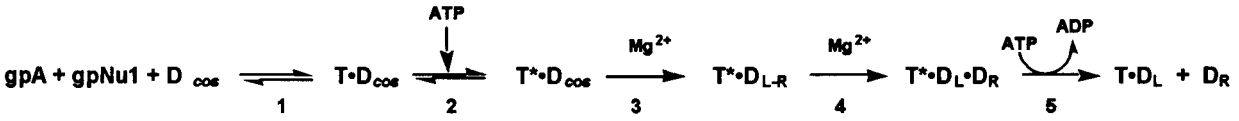

duplex nicked at the N1 site, but with an intact N2 nick site. Interestingly, mutation of cosNR similarly decreases the extent of the nuclease reaction in the absence of *cosB*. Thus, presumed abortive nicking at either *cosN* half-site leads to the formation of an abortive nicking complex, and a limited extent of the reaction. In the presence of *cosB*, the *cosN* $G_{11}C$ mutation has no effect, again demonstrating that *cosB* masks the effects of cosNR mutations.

Ultimately, it is likely that the *cosN* G_2C mutation affects multiple steps in the catalytic pathway, including gpA binding, the conformational change, and duplex nicking. Our data do not allow us to clearly define the extent to which each step is affected by the *cosN* G_2C mutation. Nevertheless, the strikingly different effects of the symmetric mutations in each *cosN* half-site clearly indicate that the two DNA substrates interact quite distinctly with terminase, and demonstrate a strong asymmetry in the nuclease reaction.

Asymmetric effects of *cosN* mutations on virus growth in vivo are observed: mutations introduced into cosNR have little effect on virus yield, while symmetrically disposed mutations in cosNL strongly affect viral development (*24*). Mutations that interfere with *cos* cleavage will limit prohead utilization and DNA packaging. Furthermore, among plaque-forming revertants of *λ cosN* $G_2C-C_{11}G$ are pseudorevertants that retain the *cosN* mutations and have a further mutation in gene *A*. One such mutant terminase was shown to have a broadened specificity; i.e., it was able to cut *cosN* $G_2C-C_{11}G$ as well as it cut *cosN*$^+$. This result implicates inefficient *cos* cleavage with the growth defects of *λ cosN* $G_2C-C_{11}G$ (*44*). The reduced burst sizes of these mutants can thus be ascribed, at least in part, to their *cos* cleavage defects.

Role of cosB in Promoting cos Cleavage Asymmetry. In contrast to the disparate results obtained with the cosNL and cosNR mutant DNA substrates in an otherwise wild-type background, deletion of *cosB* strongly attenuates the observed asymmetry. Thus, mutations introduced into either half-site have equal impacts on nuclease activity. These results provide direct evidence that *cosB* is responsible for promoting the nuclease asymmetry. Additional *λ* sequences flanking *cosN* also play a role, however, as deletion of these sequences is required to completely abolish asymmetry. It is unclear which flanking sequences of the Δ*cosB* DNAs contribute to asymmetry. An obvious candidate is *cosQ*, located to the left of *cosN*; however, extensive studies uncovered no role for *cosQ* in packaging initiation or in the *cos* cleavage reaction (*6*, *38*). It is possible that the segment between *cosN* and *cosB*, called I2, plays a role. I2 provides correct spacing between *cosN* and *cosB*, but no other function of I2 in packaging initiation has been identified (*36*).

A Model for Terminase Assembly at cos. Understanding the nature of terminase's interactions with *cosN* and *cosB* is crucial to understanding packaging initiation. Features of terminase-mediated *cos* cleavage relative to this work follow. First, terminase is a heteromultimer of gpA and gpNu1 subunits isolated as a holoenzyme complex of $gpA_1{\cdot}gpNu1_2$ protomers (*35*, *45*, *46*). Second, the staggered nicks introduced by terminase are likely made by symmetrically disposed gpA subunits whose dyad structure matches the 2-fold rotational symmetry of *cosN* (*1*, *11*, *19*, *47*). Finally, *cosB* is viewed as functioning with a gpNu1 oligomer to form a specialized nucleoprotein complex which in turn promotes gpA assembly at *cosN*. We suggest the following model to account for the data presented here and in the literature. Central to duplex nicking is the assembly of a gpA dimer symmetrically bound to *cosN*. Assembly is mediated by intrinsic binding interactions between the gpA subunits and the *cosN* half-sites and, less critically, cooperative binding interactions between the gpA subunits (*5*; Figure 5). Additionally, assembly of gpA at the cosNR half-site is strongly influenced by cooperative binding interactions with gpNu1 assembled at *cosB*. Thus, mutations in the cosNR half-site are masked by higher order binding interactions, and neither gpA assembly nor duplex nicking is appreciably affected. Indeed, virus assembly in vivo is unaffected by these mutations. Conversely, intrinsic gpA·cosNL binding interactions play a major role in assembling the nicking complex at this half-site, and mutations in cosNL have striking effects. In the absence of *cosB*, cooperative gpNu1 binding interactions are absent, and intrinsic binding interactions between the gpA subunits and both *cosN* half-sites are responsible for assembly of a symmetrically disposed nuclease dimer. In this case, mutations in either half-site have equal impacts on interactions between terminase and *cosN*. Assembly steps become rate-limiting, duplex nicking is impaired, and virus development is affected.

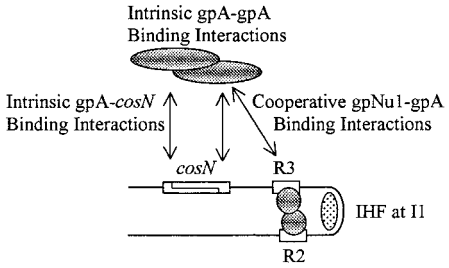

FIGURE 5: Terminase interactions at *cos*. Depicted are intrinsic interactions of gpA subunits (large shaded ellipses) with *cosN* half-sites, and cooperative interactions of gpA subunits with gpNu1 subunits (shaded circles) bound at *cosB*. Binding of a gpNu1 dimer with the R3 and R2 sequences of *cosB* is shown along with IHF (dotted ellipse) binding to I1. gpNu1 binding to R1 is not shown. See text for details.

In summary, gpNu1 stimulates nuclease activity by the *cosB*-dependent formation of an activated nuclease complex, which depends on the highly ordered oligomerization of gpNu1 on the three R sites of *cosB*. Because *cosB* properly positions the terminase protomer binding to cosNR, this interaction is unaffected by the *cosN* $C_{11}G$ mutation in cosNR. The protomer on cosNL has no adjacent supporting site, however, so the *cosN* G_2C mutation destabilizes the complex required for efficient cleavage. This model is consistent with the observations that (i) *cosB* aids N1 nicking to a greater extent than N2 nicking (*36*, *38*), and (ii)

substrates with point mutations in the R sites of *cosB* only mildly affect cosNL nicking, while cosNR nicking is obviously impaired (*38*). These studies suggest a link between *cosB* and nicking at the cosNR half-site. The studies presented here confirm that *cosB* is indeed responsible for asymmetry in the nuclease reaction.

The terminase−*cos* system shows how the interaction of a bivalent DNA binding protein with one binding site can be influenced by interactions with the other binding site. In the present case, the interactions of gpA with rotationally symmetric *cosN* are rendered asymmetric by the interactions of gpNu1 with the *cosB* R sites. Other examples exist, such as in the λ site-specific recombination system. The recombinase protein integrase binds the symmetric core of the phage attachment site, *attP*, and additionally binds flanking arm-type sequences to form an asymmetric nucleoprotein structure that captures the bacterial chromosome's *attB* site. Recombination is initiated by cleavage and exchange of the top strands of the phage and bacterial *att* site core sequences (*46*). The top strand bias in strand exchange is not determined by the core region of the attachment site, but rather depends on the arrangement of the flanking arm-type sequences. Asymmetric *cosN* cleavage is similarly mediated by an asymmetric nicking complex composed of terminase gpA and gpNu1 subunits. This asymmetric complex imparts efficient and accurate nicking, followed by unidirectional DNA packaging (*5*, *25*, *37*, *38*, *40*, *41*).

ACKNOWLEDGMENT

We thank our co-workers Alok Dhar, Carol Duffy, Young Hwang, Jean Sippy, and Doug Wieczorek for their interest and advice during the course of this work. Andy Becker, as usual, gave us encouragement and helpful comments.

REFERENCES

1. Becker, A., and Murialdo, H. (1990) *J. Bacteriol. 172,* 2819−2824.
2. Fujisawa, H., and Hearing, P. (1994) *Semin. Virol. 5,* 5−13.
3. Roizman, B., and Sears, A. E. (1991) in *Fundamental Virology* (Fields, B. N., Knipe, D. M., and Chanock, R. M., Eds.) pp 863−865, Raven Press, New York.
4. Feiss, M., Widner, W., Miller, G., Johnson, G., and Christiansen, S. (1983) *Gene 24,* 207−218.
5. Yang, Q., Hanagan, A., and Catalano, C. E. (1997) *Biochemistry 36,* 2744−2752.
6. Cue, D., and Feiss, M. (1993) *Proc. Natl. Acad. Sci. U.S.A. 90,* 9290−9294.
7. Feiss, M., Kobayshi, I., and Widner, W. (1983) *Proc. Natl. Acad. Sci. U.S.A. 80,* 955−959.
8. Shinder, G., and Gold, M. (1988) *J. Virol. 62,* 387−392.
9. Miwa, T., and Matsubara, K. (1983) *Gene 24,* 199−206.
10. Bear, S., Court, D., and Friedman, D. (1984) *J. Virol. 52,* 966−972.
11. Feiss, M. (1986) *Trends Genet. 2,* 100−104.
12. Kypr, J., and Mrazek, J. (1986) *J. Mol. Biol. 91,* 139−140.
13. Shinder, G., and Gold, M. (1989) *Nucleic Acids Res. 17,* 2005−2022.
14. Xin, W., and Feiss, M. (1988) *Nucleic Acids Res. 16,* 2015−2030.
15. Xin, W., and Feiss, M. (1993) *J. Mol. Biol. 230,* 492−504.
16. Xin, W., Cai, Z.-H., and Feiss, M. (1993) *J. Mol. Biol. 230,* 505−515.
17. Kosturko, L., Daub, E., and Murialdo, H. (1989) *Nucleic Acids Res. 17,* 329−334.
18. Rice, P. A., Yang, S., Mizuuchi, K., and Nash, H. A. (1996) *Cell 87,* 1295−1306.
19. Catalano, C. E., Cue, D., and Feiss, M. (1995) *Mol. Microbiol. 16,* 1075−1086.
20. Mendelson, I., Gottesman, M., and Oppenheim, A. B. (1991) *J. Bacteriol. 173,* 1670−1676.
21. Davidson, A., and Gold, M. (1992) *Virology 161,* 305−315.
22. Rubinchik, S., Parris, W., and Gold, M. (1994) *J. Biol. Chem. 269,* 13575−13585.
23. Catalano, C. E. (2000) *Cell Mol. Life Sci. 57,* 128−148.
24. Xu, S. Y., and Feiss, M. (1991) *J. Mol. Biol. 220,* 281−292.
25. Higgins, R. R., and Becker, A. (1994) *EMBO J. 13,* 6152−6161.
26. Daniels, D., Schroeder, J., Szybalski, W., Sanger, F., Coulsen, A., Hong, D., Hill, D., Peterson, G., and Blattner, F. (1983) in *Lambda II* (Hendrix, R. W., Roberts, J. W., Stahl, F. W., and Weisberg, R. A., Eds.) pp 519−676, Cold Spring Harbor Laboratory Press, Cold Spring Harbor, NY.
27. Arber, W., Enquist, L., Hohn, B., Murray, N. E., and Murray, K. (1983) in *Lambda II* (Hendrix, R. W., Roberts, J. W., Stahl, F. W., and Weisberg, R. A., Eds.) pp 433−366, Cold Spring Harbor Laboratory Press, Cold Spring Harbor, NY.
28. Sambrook, J., Fritsch, E. F., and Maniatis, T. (1989) in *Molecular Cloning, A Laboratory Manual*, Appendix A, Cold Spring Harbor Laboratory Press, Cold Spring Harbor, NY.
29. Kunkel, T. A. (1985) *Proc. Natl. Acad. Sci. U.S.A. 82,* 488−492.
30. Six, E. W., and Klug, C. A. C. (1973) *Virology 51,* 327−344
31. Wiman, M., Bertani, G., Kelly, B., and Sasaki, I. (1971) *Mol. Gen. Genet. 107,* 1−31.
32. Chow, S., Daub, E., and Murialdo, H. (1987) *Gene 60,* 277−289.
33. Hanahan, D. (1983) *J. Mol. Biol. 166,* 557−580.
34. Hwang, Y., and Feiss, M. (1995) *Virology 211,* 367−376.
35. Tomka, M. A., and Catalano, C. E. (1993) *J. Biol. Chem. 268,* 3056−3065.
36. Higgins, R. R., Lucko, H. J., and Becker, A. (1988) *Cell 54,* 765−775.
37. Cue, D., and Feiss, M. (1992) *J. Mol. Biol. 228,* 58−71.
38. Cue, D., and Feiss, M. (1993) *J. Mol. Biol. 234,* 594−609.
39. Becker, A., Murialdo, H., and Gold, M. (1977) *Virology 78,* 291−305.
40. Higgins, R. R., and Becker, A. (1994) *EMBO J. 13,* 6162−6171.
41. Woods, L., Terpening, C., and Catalano, C. E. (1997) *Biochemistry 36,* 5777−5785.
42. Higgins, R. R., and Becker, A. (1995) *J. Mol. Biol. 252,* 31−46.
43. Wieczorek, D., and Feiss, M. (2001) *Genetics 158,* 495−506.
44. Arens, J. S., Hang, Q., Hwang, Y., Tuma, B., Max, S., and Feiss, M. (1999) *J. Bacteriol. 181,* 218−224.
45. Gold, M., and Becker, A. (1983) *J. Biol. Chem. 258,* 14619−14625.
46. Parris, W., Rubinchik, S., Yang, Y. C., and Gold, M. (1994) *J. Biol. Chem. 269,* 13564−13574.
47. Murialdo, H. (1991) *Annu. Rev. Biochem. 60,* 125−153.
48. Kitts, P. A., and Nash, H. A. (1988) *J. Mol. Biol. 204,* 95−107.

BI011126R